The Nature of Power Saturation in Traveling Wave Tubes

By C. C. CUTLER

(Manuscript received February 2, 1956)

The non-linear operating characteristics of a traveling wave tube have been studied using a tube scaled to low frequency and large size. Measurements of electron beam velocity and current as a function of RF phase and amplitude show the mechanism of power saturation.

The most important conclusions are:

I. There is an optimum set of parameters ($QC = 0.2$ and $\gamma r_0 = 0.5$) giving the greatest efficiency.

II. There is a best value of the gain parameter "C" which leads to a best efficiency of about 38 per cent.

III. A picture of the actual spent beam modulation is now available which shows the factors contributing to traveling wave tube power saturation.

INTRODUCTION

The highest possible efficiency of the traveling wave tube has been estimated from many different points of view. In his first paper on the subject[1] J. R. Pierce showed that according to small signal theory, when the dc beam current reaches 100 per cent modulation an efficiency of

$$\eta = \frac{C}{2} \tag{1}$$

is indicated,* and thus the actual efficiency might be limited to something like this value. Upon later consideration[2] he concluded that the ac convection current could be twice the dc current and that one might expect an efficiency of

$$\eta = 2C \tag{2}$$

He also considered the effects of space charge, and concluded on the

* Symbols are consistent with Reference 2 and are listed at the end of this paper.

same basis that under high space charge and elevated voltage conditions, efficiencies might be as high as

$$\eta = 8C \tag{3}$$

J. C. Slater[3] on the other hand considered the motion of electrons in a traveling wave and concluded that the maximum possible reduction in beam velocity would also indicate a limiting efficiency of $2C$. Taking a more realistic account of the electron velocity, Pierce[2] showed that these considerations lead to a value of

$$\eta = -4y_1C \tag{4}$$

which, since y_1 ranges between $-\frac{1}{2}$ and -2, leads to the same range of values as the other predictions.

None of these papers purport to give a physical picture of the overloading phenomenon, but only specify clear limitations to the linear theory. L. Brillouin[4] on the other hand found a stable solution for the flow of electrons bunched in the troughs of a traveling wave. This he supposed to represent the limiting high level condition of traveling wave tube operation. His results give an efficiency of

$$\eta = 2bC \tag{5}$$

In the first numerical computations of the actual electron motion in a traveling wave tube in the nonlinear region of operation, Nordsieck[5] predicted efficiencies ranging between 2.5 and 7 times C and showed that there would be a considerable reduction in efficiency for large diameter beams, due to the non-uniformity of circuit field across the beam diameter. He also gave some indication of the electron dynamics involved. Improving on this line of attack, Poulter[6] calculated some cases including the effect of space charge and large values of C.

Tien, Walker and Wolontis[7] carried computations still further for small values of C by including the effect of small beam radii upon the space charge terms, and showed that space charge and finite (small) beam radii result in much smaller efficiencies than were previously predicted. J. E. Rowe[8] got similar results and gave more information on the effects of finite values of C. Computations for large values of C by Tien[9] showed that a serious departure from the small C conditions takes place above values of $C = 0.1$ if space charge is small (i.e., below $QC = 0.1$) and above $C = 0.05$ for larger values of space charge. They indicated that a maximum value of efficiency as high as 40 per cent should be possible using $C = 0.15$, $QC = 0.1$ and elevated beam voltages.

These five papers give some insight into the electron dynamics of power

saturation, but still involve questionable approximations which make it desirable to compare predictions with the actual situation.

Theoretical considerations of the effects of attenuation upon efficiency have not led to conclusions coming even close to the observed results. Measured characteristics[10, 11] show that the effect of attenuation is very large, but that attenuation may be appropriately distributed to attain stability and isolation between input and output of the tube without degrading the output power.

There are also several papers in the French and German periodicals which deal with the question of traveling wave tube efficiency. Some of these are listed in References 12 through 20.

This paper describes measurements of efficiency and of beam modulation made on a traveling wave tube scaled to large size,* and low frequencies. The construction of the tube, shown in Fig. 1, and the measurement of its parameters were much more accurate than is usual in the design of such tubes. The results are believed to be generally applicable to tubes having similar values of the normalized parameters.

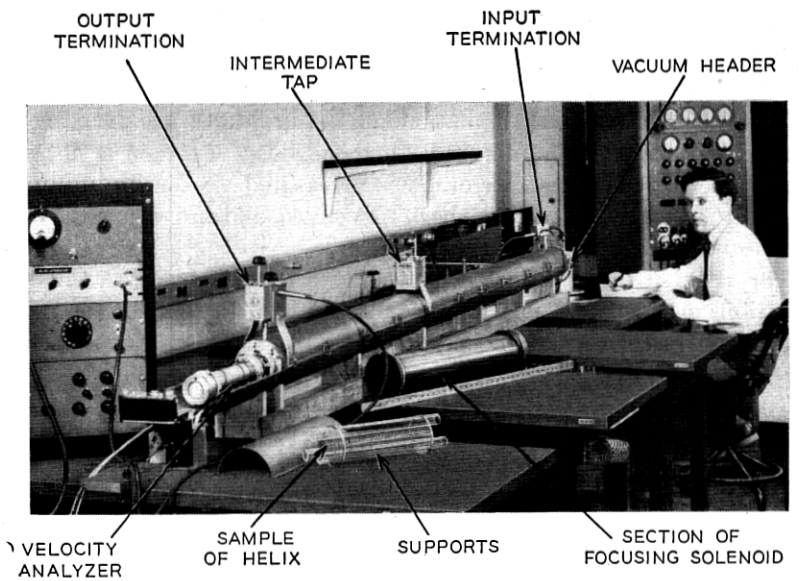

Fig. 1 — The scale model traveling wave tube. The tube is 10 feet long with a copper helix supported by notched glass tubing from an aluminum cylinder overwound with a focusing solenoid. It is continuously pumped and readily demountable.

* See Appendix.

Two kinds of measurements are described. First, the efficiency and power output are determined for various conditions of operation, and second the spent beam ac velocity and current are measured. The principal results are shown in Figs. 2 to 4 which give the obtainable efficiencies, and in Figs. 7 to 10 which show some of the factors which contribute to power saturation. These figures are discussed in detail later. The most significant phenomenon is the early formation of an out-of-phase bunch of electrons which have been violently thrown back from the initial bunch, absorbing energy from the circuit wave, and inhibiting its growth. The final velocity of most of the electrons is near to that of the circuit wave which would lead to a value of

$$\text{limiting efficiency } \eta = -2y_1C \tag{6}$$

if the wave velocity maintained its small signal value. Actually the wave slows down, under the most favorable conditions giving rise to a somewhat higher efficiency. For other conditions, space charge, excess electron velocity, or nonuniformity of the circuit field enter in various ways to prevent the desired grouping of electrons and result in lower efficiencies.

The observed efficiencies are a rather complicated function of QC, γr_0 and C. To compare with efficiencies obtained from practical tubes one must account for circuit attenuation and be sure that some uncontrolled factor such as helix non-uniformity and secondary emission is not seriously affecting the tubes' performance. Measured efficiencies of several carefully designed tubes have been assembled and are compared with the results of this paper in Table I.

The results of these measurements compare favorably with the computations of Tien, Walker and Wolontis[7], and of Tien[9]. There are, however some important differences which are discussed in a later section.

TRAVELING WAVE TUBE EFFICIENCY MEASUREMENTS

Reasoning from low level theory, efficiency should be a function of the gain parameter, "C," the space charge parameter "QC," the circuit attenuation, and (for large beam sizes), the relative beam radius "γr_0." It was soon found that efficiency is a much more complicated function of γr_0 than expected. The initial objective was to determine the effect of QC, C, and γr_0 separately on efficiency, but it was necessary to give a much more general coverage of these parameters, not assuming any of them to be small.

Most of the measurements have been made with small values of loss

TABLE I

Laboratory	Freq. mc.	QC	γr_0	C	η measured	η (from Fig. 3)	η (From Fig. 3 with allowance for circuit attenuation[10]
McDowell*	4,000	0.27	0.62	0.078	**19.5**	26	**21.6**
	6,000	0.29	0.8	0.058	**13.2**	16.2	**12.5**
Brangaccio and Cutler†	4,000	0.61	0.87	0.041	**11**	6	**6**
Danielson and Watson*	11,000	0.35	1.2	0.05	**6.6**	7	**4.8**
R. R. Warnecke[16, 17, 18]	870	0.32	0.3	.125	**27**	33	**33**
W. Kleen and W. Friz[15]	4,000	0.5	0.43	0.05	**7.8**	11.5	**5.7**
W. Kleen‡	4,000	0.2	0.94	0.1	**20**	26	**22**
L. Brück§	3,500	0.19	0.6	0.065	**15**	23	**18.5**
Hughes Aircraft Co.	3,240	0.19	0.94	0.12	**39**	31	**29**
	9,000	0.15	1.3	0.11	**25**	15.5	**12.7**

* At Bell Telephone Laboratories.
† Reference 10 (a slight beam misalignment could account for most of this difference).
‡ Siemens & Halske, Munich, Germany.
§ Telefunken, Ulm, Germany.

and of the gain parameter, where efficiency is proportional to C, as expected from small-signal small-C predictions. This reduces the problem to a determination of η/C versus QC and γr_0.

Many measurements of this kind have been made, and the data are summarized in Figs. 2 and 3, with efficiency shown as a function of QC and γr_0. In Fig. 2 we have the efficiency when the beam voltage is that which gives maximum low-level gain. Fig. 3 shows the efficiency obtained when the beam potential is raised to optimize the power output, and contours of constant efficiency have been sketched in. There is significantly higher efficiency than before in the region of maximum efficiency, but not much more elsewhere.

Fig. 4 shows how efficiency varies with C for a small value of QC, a representative value of γr_0, and with beam voltage increased to maximize the output. This indicates a maximum of about 38 per cent at $C = 0.14$.

Some of the computed results of Tien, Walker and Wolontis,[7] and of Tien[9] are also indicated in the figures. Their results generally indicate somewhat greater efficiencies than were observed, but in the most significant region the comparison is not too bad as will be seen in a later section.

The measurements are for conditions having negligible circuit loss near the tube output. There are no new data on the effect of loss, but earlier results[10] have been verified by measurements at Stanford University[11] and are still believed to be a satisfactory guide in tube design.

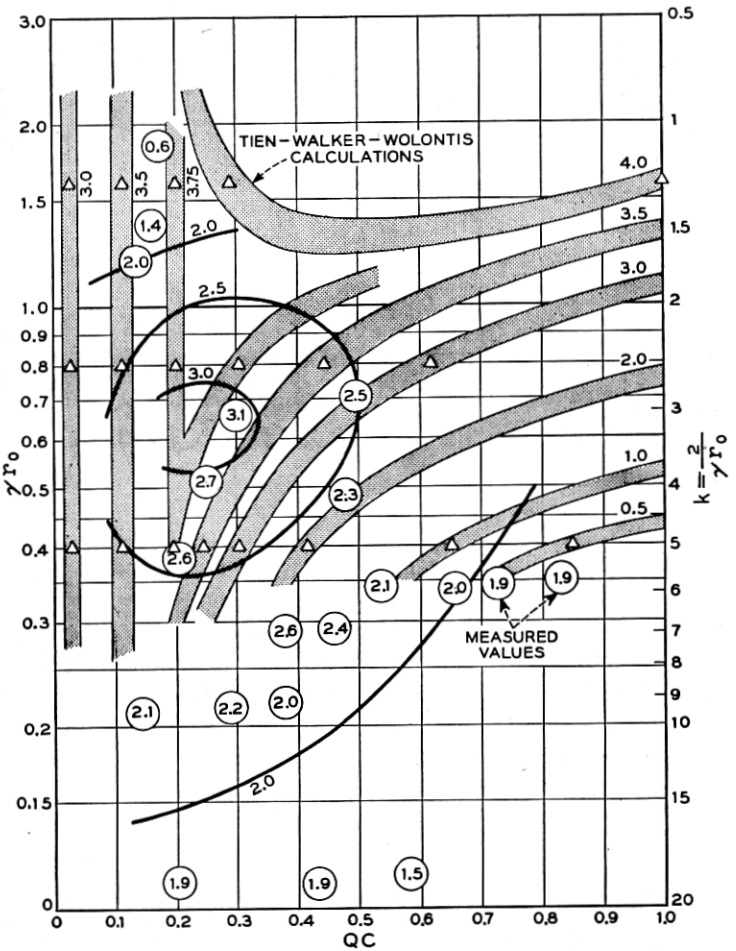

Fig. 2 — Values of efficiency/C as a function of QC and γr_0 at the voltage giving maximum gain per unit length. The shaded contours and triangular points are from the computations[7] of Tien, Walker and Wolontis. The circled points are from the measurements and the line contours are estimated lines of constant efficiency. The most significant difference is for large beam radii, where the RF field varies over the beam radius in a way not accounted for in the computations.

SPENT BEAM CHARACTERISTICS

The scale model traveling wave tube was followed by a velocity analyzer as sketched in Fig. 5 and described in the Appendix. A sample of the beam at the output end of the helix is passed through a sweep circuit to separate electrons according to phase, and crossed electric and

magnetic fields to sort them according to velocity. The resulting beam draws a pattern on a fluorescent screen as shown in Fig. 6 from which charge density and velocity can be measured as a function of signal phase. The velocity coordinate is determined by photographing the ellipse with several different beam potentials, as in Fig. 6(a), and the phase coordinate is measured along the ellipse. From pictures like this a complete determination of electron behavior is obtained from the linear region up to and above the saturation level.

The results of such a run are plotted in Fig. 7. The upper lefthand

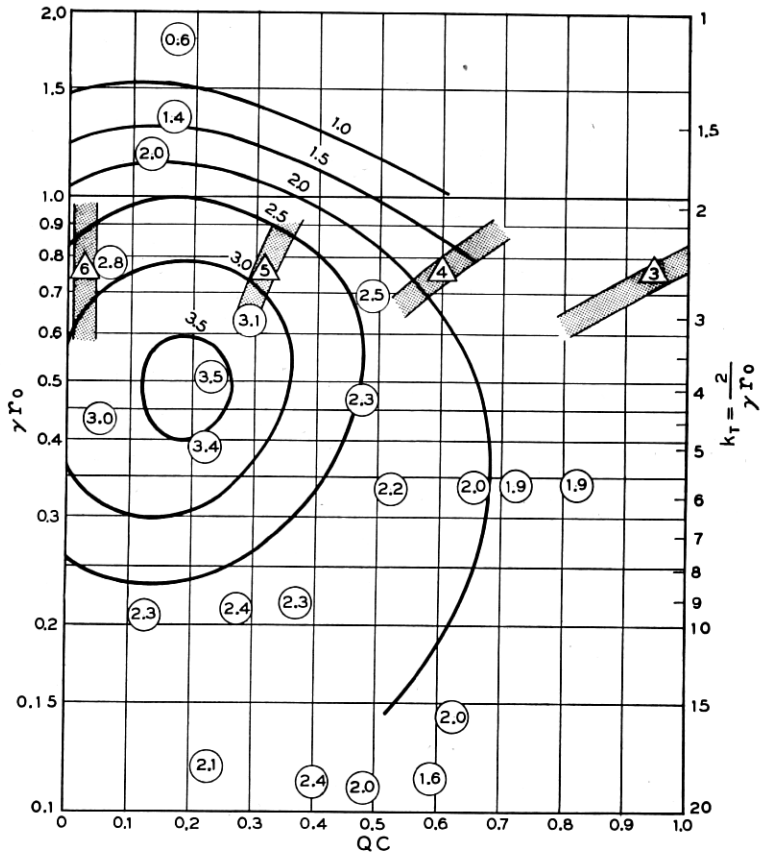

Fig. 3 — Values of efficiency/C as a function of QC and γr_0 at elevated beam voltage. Raising the beam voltage has little effect at large QC and small γr_0, and less than expected anywhere. Again the triangular points are from Tien, Walker and Wolontis,[7] and the line contours are estimated from the measured data.

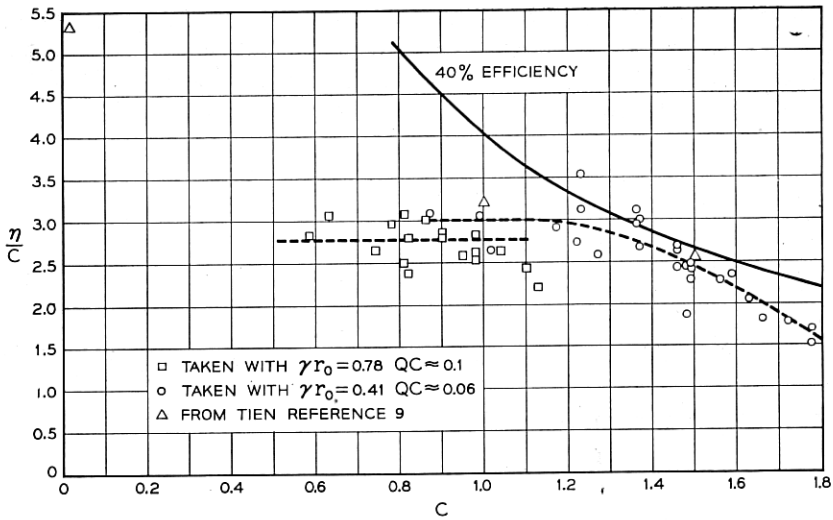

Fig. 4 — Efficiency/C for large values of C and with elevated beam voltage. Efficiency seriously departs from proportionality to C at $C = 0.14$, where a maximum efficiency of about 38 per cent is measured.

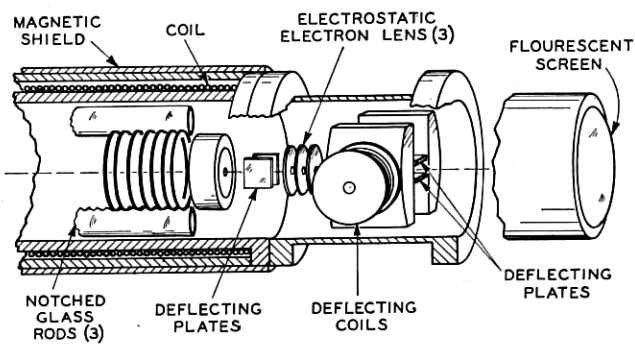

Fig. 5 — The velocity analyzer. A sample of the spent electron beam is accelerated to a high potential, swept transversely with a synchronous voltage, sorted with crossed electric and magnetic fields, and focused onto a fluorescent screen.

pattern, Fig. 7(a), is representative of the low level (linear) conditions (22 db below the drive for saturation output). The dashed curve represents the voltage on the circuit, inverted so that electrons can be visualized as rolling down hill on the curve. The phase of this voltage relative to the electron ac velocity is computed from small signal theory, but

everything else in Fig. 7, including subsequent variations of phase, are measured. The solid line patterns represent the ac velocity, and the shaded area, the charge density corresponding to that velocity. Thus in each pattern we have a complete story of (fundamental) circuit voltage, electron velocity and current density as a function of phase, for a particular signal input level. The velocity and current modulations at small signal levels check calculated values well, and it is not difficult to visualize the dynamics giving this pattern.

Consider first the situation in the tube at small signal amplitudes. At the input an unmodulated electron beam enters the field of an electromagnetic wave moving with approximately the same velocity as the electrons. The electrons are accelerated or decelerated depending upon their phase relative to the wave, and soon are modulated in velocity. The velocity modulation causes a bunching of the electrons near the potential maxima (i.e., the valleys in the inverted potential wave shown) and these bunches in turn induce a new electromagnetic wave component onto the circuit roughly in quadrature following the initial wave. The addition of this component gives a net field somewhat retarded from the initial wave and larger in amplitude. Continuation of this process

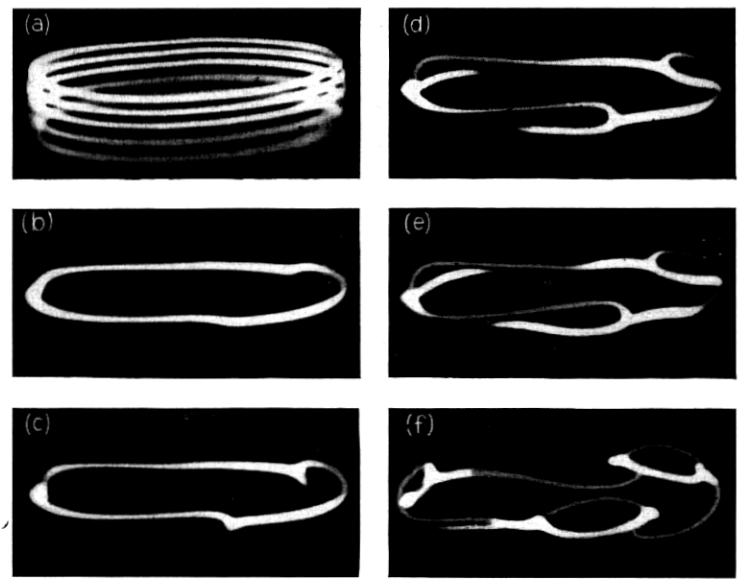

Fig. 6 — Velocity analyzer patterns. The beam sample is made to traverse an ellipse at ⅓ the signal frequency. Current density modulation appears as intensity variation, and velocity variation as vertical deflection from the ellipse.

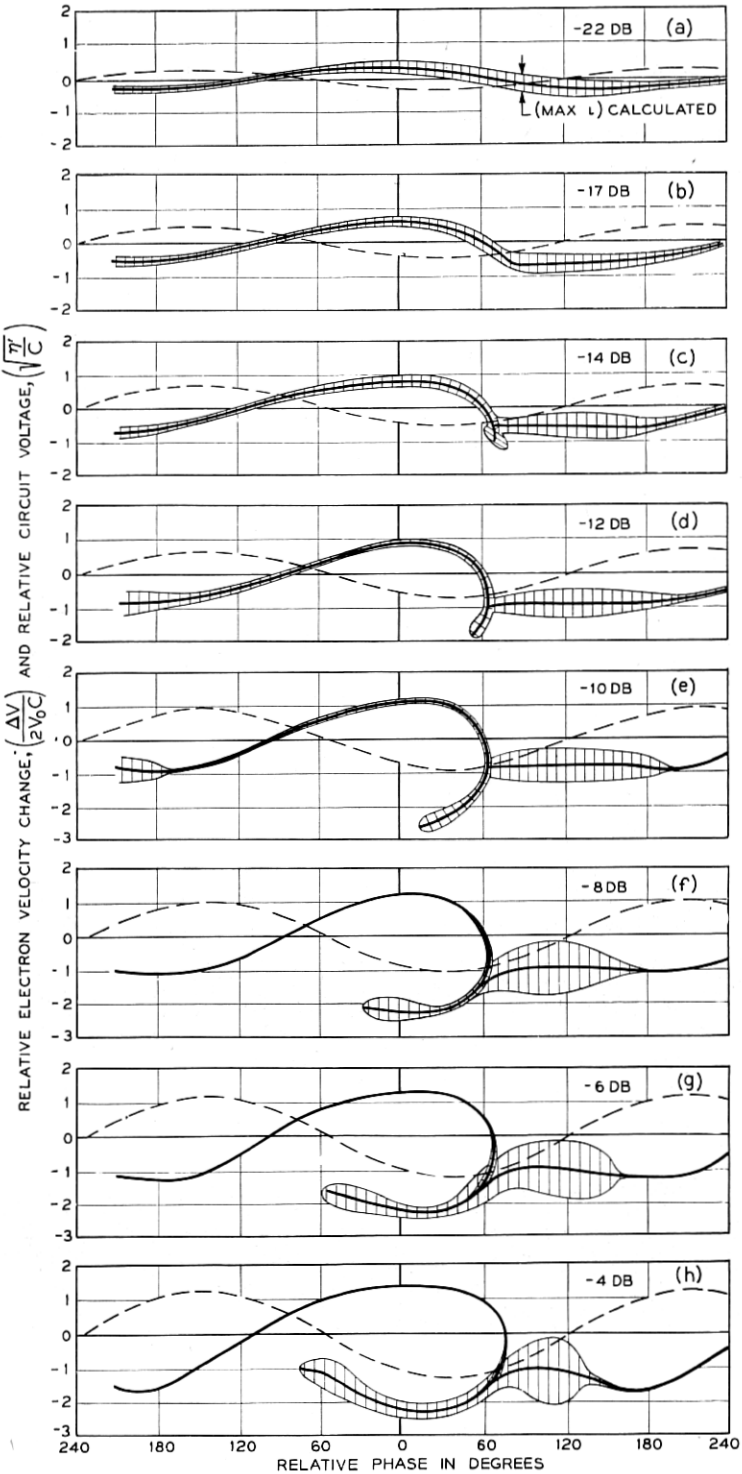

Fig. 7 — Curves of current and velocity as a function of phase for various input levels. The velocity becomes multivalued at a very low level, a tail forming a nucleus for a second electron bunch which eventually caused saturation in the output. For this run $C = 0.1$ Q,$C = 0.06$, $\gamma r_0 = 0.4$ and $b = 0.26$.

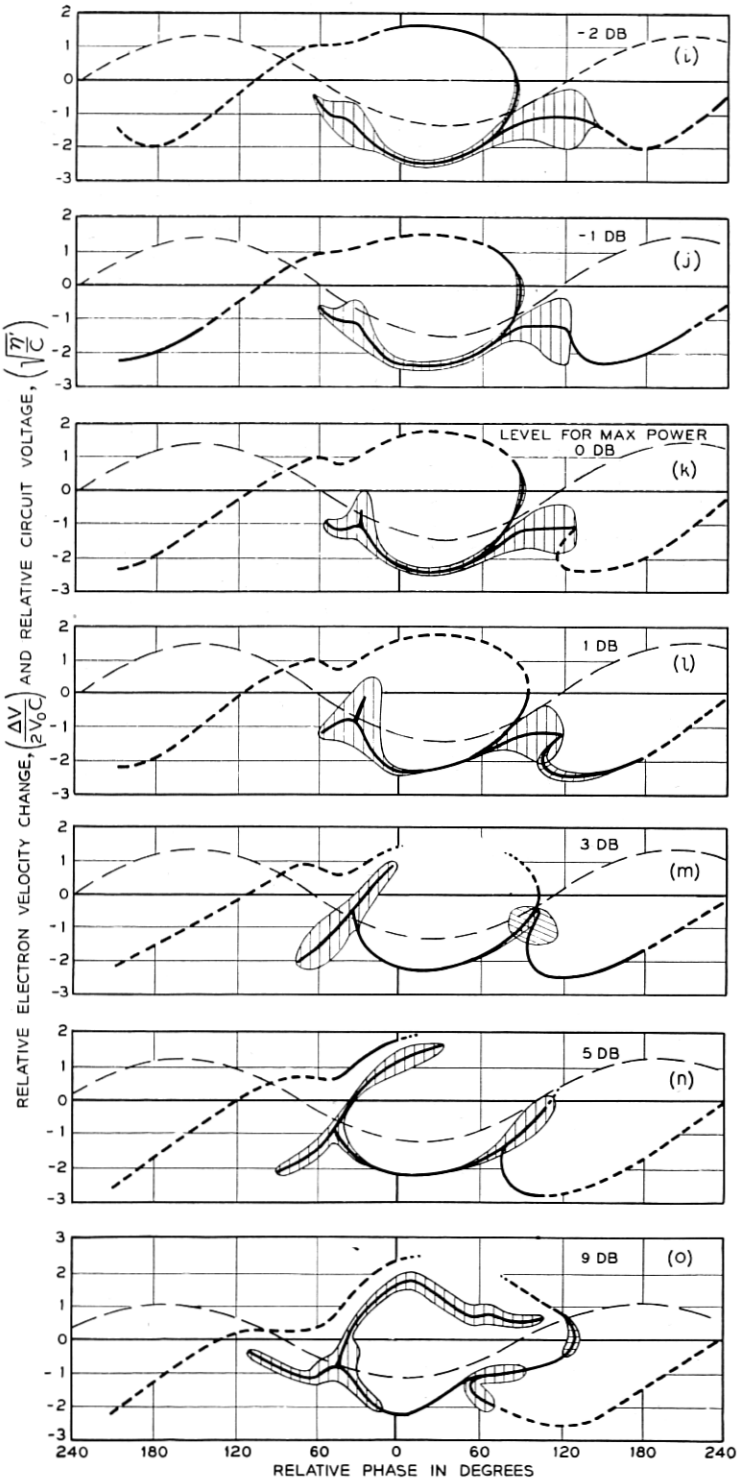
-2 DB
(i)
-1 DB
(j)
LEVEL FOR MAX POWER
0 DB
(k)
1 DB
(l)
3 DB
(m)
5 DB
(n)
9 DB
(o)
RELATIVE ELECTRON VELOCITY CHANGE, $\left(\frac{\Delta V}{2V_0C}\right)$ AND RELATIVE CIRCUIT VOLTAGE, $\left(\sqrt{\frac{M}{C}}\right)$
RELATIVE PHASE IN DEGREES
240 180 120 60 0 60 120 180 240

may be seen to give a resultant increasing wave traveling somewhat slower than the initial wave, and thus slower than the electron velocity. Returning to Fig. 7 we see that electrons in the decelerating field [from +30 to +210° in Fig. 7(a)] have been slowed down, and because of their initial velocity being faster than the wave velocity, have moved forward in the wave giving a region of minimum velocity somewhat in advance of the point of maximum retarding field (greatest negative slope in the wave potential). Also, bunching due to acceleration and deceleration of electrons has produced a maximum of electron current density which, because of the initial excess electron velocity, is somewhat to the right of the potential maximum (downward).

As the level is increased the modulation increases and at 17 db below saturation drive, Fig. 7(b), some nonlinearity is evident. The velocity and current are no longer sinusoidal, but show the beginnings of a cusp in the velocity curve and a definite non-sinusoidal bunching of the electrons in the retarding field region (between +30 and 210°).

In the next pattern, Fig. 7(c), at 14 db below saturation a definite cusp has formed with a very sharp concentration of electrons extending significantly below the velocities of the other electrons. We already have a wide range of velocities in the vicinity of the cusp, and at this level the single valued velocity picture of the traveling wave tube breaks down. Although it cannot be distinctly resolved, the study of many such pictures leaves little doubt that the cusp and its later development is really a folding of the velocity line.

The next pattern at 12 db below saturation drive, Fig. 7(d), shows a greater development of the spur and a somewhat greater consolidation of current in the main bunch between +60° and +180°. It is interesting that the velocity in this region has not changed significantly. In order for this to be true the space charge field must just compensate for the circuit field. In the vicinity of the 60° point the space charge field obviously must reverse, accounting for the very sharp deceleration evident in the very rapid development of the low velocity spur. The decelerating field must be far from that of the wave, inasmuch as the electrons just behind the cusp are much more sharply decelerated than those preceding the cusp. We conclude that there are very sharply defined space charge fields much stronger than the helix field. At this relatively low drive, the velocity spread has already achieved its maximum peak value.

The succeeding three patterns show a continuing growth of the spur, a continued bleeding of electrons from the higher velocity regions, and a consolidation of the main bunch just in advance of the spur. Presumably the increased concentration of space charge in the bunch has kept

pace with the increasing helix field, so that the net decelerating field still balances to nearly zero. At 4 db below the saturation drive, Fig. 7(h), the spur has moved well into the accelerating region, and has been speeded up. The main bunch of electrons is still to the right of the spur, and has been consolidated into a 60° interval. The few electrons in advance of this region evidently no longer find the space charge field sufficient to balance the circuit field, and are being decelerated into a second low velocity loop.

The next three patterns show a continued growth of this second low velocity loop, further consolidation of the 'main bunch', and the rapid formation of a second bunch in the accelerating field at the end of the spur. It is interesting that at saturation drive, Fig. 7(k) the two bunches are very nearly equal, and in equal and opposite circuit fields, nearly 180° apart. The reason for the saturation is that while the main bunch is still giving up energy to the wave, the new one is absorbing energy at an equal rate. The fundamental component of electron current is evidently small, and is in quadrature with the circuit field. The current density in the dashed regions is less than 1 per cent of that in the bunches, and probably more than 95 per cent of the electrons are in the two bunches. Two new effects are observable at this level. The second electron bunch has begun to come apart, presumably because of strong localized space charge forces. These forces are also evident in the kink in the velocity pattern drawn by the fast electrons at the same phase as the second bunch.

Since the majority of the current is in the two bunches at a reduced velocity of

$$\frac{\Delta V}{2V_0C} = -1.1$$

one would expect an output efficiency of

$$\frac{\Delta V}{V_0} = 2.2C$$

The actual measured efficiency

$$\frac{\text{RF power output}}{\text{DC power input}}$$

was 2.0 C. Under the conditions described, (6) would give 1.4 C.

At still higher drive levels the pattern continues to develop, electrons from the first bunch falling back into the second, which in turn continues to divide, one part accelerating ahead into a new spur, and the other

slowing down and falling further back in phase. At 9 db above saturation, Fig. 7(o), the pattern is quite complex, and at still higher levels it is utterly indescribable.

It is interesting that the velocity gives a line pattern, even though a multivalued one. It is reasonable to suppose that the development of the spur is really a folding of the velocity line so that the spur is really a double line. Thus, at the 9 db level, and at 0° phase, for instance, there must be electrons originating from five different parts of the initial distribution. In an attempt to verify this the resolution of the velocity analyzer was adjusted so that a difference in velocity of 2 per cent of the overall spread could be observed, but there was no positive indication of more than one velocity associated with any line shown.

There has been a long-standing debate as to whether or not electrons are trapped in the circuit field, or continue to override the wave at large amplitudes. The observations indicate that with low values of space charge and near synchronous voltage the electrons are effectively trapped in the wave until well above saturation amplitude. In other circumstances this is not the case, as we shall see.

SPACE CHARGE EFFECTS

The data of Fig. 7 were taken with a very small value of the space charge parameter QC, so small in fact as to be almost negligible as far as low level operation is concerned. Yet the space charge forces evidently played a very strong role in the development of the velocity and current patterns. It is doubtful that space charge would ever be negligible in this respect, because if the space charge parameter were smaller, the bunching would be more complete, the electron density in the bunch would be greater limited only by the balance of space charge field and circuit field in the bunch. The effect of decreasing QC further therefore is a greater localization of the space charge forces, rather than a reduction of their magnitude, at least until the bunch becomes short compared to the beam radius.

Increasing the value of the space charge parameter has quite the opposite effect. In Fig. 8 are shown three velocity-current distributions at the saturation level, for different values of QC. It can be seen that a result of increased space charge is a greater spread of velocities, and a wider phase distribution of current.

With the introduction of space charge, the velocity difference between the electrons and the circuit wave at low levels is increased. Consequently electrons spend a longer time in the decelerating field before being thrown back in the low velocity spur, and thus lose more energy. The

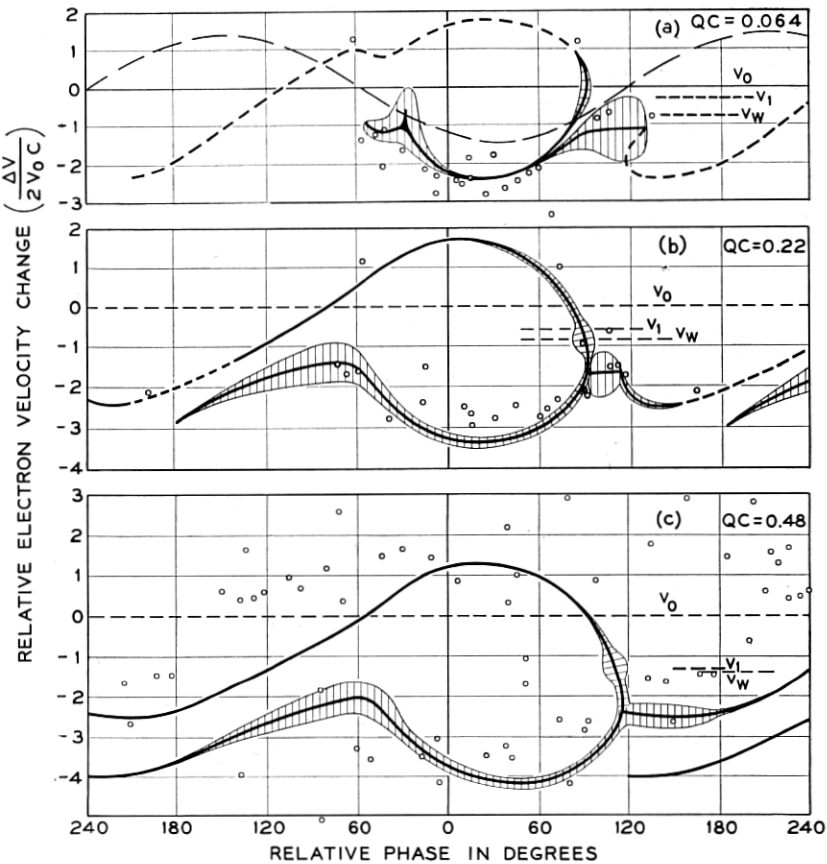

Fig. 8 — A comparison showing the effect of the space charge parameter QC on the velocity and current at overload. The points represent the disc electrons of the computations[7] of Tien, Walker and Wolontis. For this run $\gamma r_0 = 0.4$ and b is chosen for maximum x_1 .

greater reduction of velocity results in a faster and farther retarding of the current in the spur before the retarded electrons recover velocity in the accelerating region. Also the larger space charge forces prevent as tight bunching of the electrons anywhere, so that at overload they are spread over a much wider phase interval (about 360° for $QC = 0.5$). Space charge also prevents electrons from the forward part of the bunch from being trapped so that more electrons escape ahead of the decelerating field and more current is found in the upper half of the velocity curve. This very likely is the reason that efficiency decreases when QC is increased above about 0.3.

EFFECT OF BEAM SIZE

In small signal operation, decreasing the beam radius below that which assures a constant circuit field throughout the beam has no effect except that accounted for by its effect on QC. Fig. 9 shows that for large signals, however, it has a pronounced effect. When the beam is made smaller (with QC maintained by changing frequency and beam current), the slowed up tail is formed at a much lower signal level (not shown), by a very few electrons which begin to collect in the accelerating region before the beam is strongly modulated. As the level is increased, the current is redistributed, more going into the tail without much alteration in the shape of the velocity pattern, and with no strong bunching at any part of the curve. This result is exaggerated in Fig. 9(c) by measuring with a

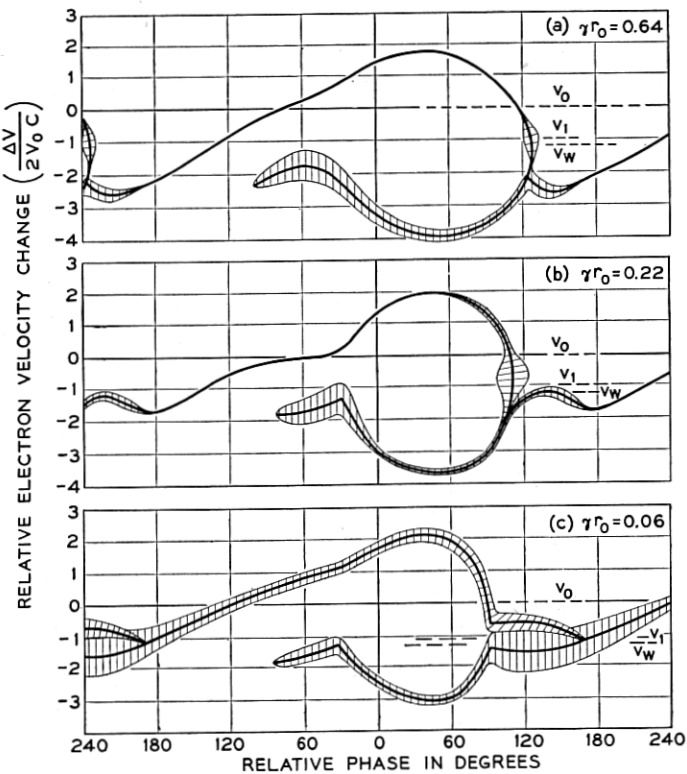

Fig. 9 — Curves of current and velocity as influenced by γr_0. Space charge becomes a very potent factor near overload, especially when the beam is small. For this run $QC = 0.34$ and $b = 1.0$.

ridiculously small beam. By comparison with curves taken for larger beams, the tail is diminutive, electrons are much more uniformly distributed over all velocities and phases, and a peculiar splitting of velocities in the main bunch is found. The latter indicates that electrons entering from the higher velocity region move forward in the bunch, and the rest gradually retard. The smaller reduction in velocities, and the spread of electrons into the higher velocity regions is consistent with the lower efficiency measured (Fig. 2).

To explain the observed difference in high level performance of tubes with different size beams we must consider the character of the ac longitudinal space charge field. The coulomb field from an elemental length of an electron beam is inversely proportional to the square of the distance from the element

$$E = \text{Const}\,\frac{q\Delta z}{(z - z_1)^2} \tag{7}$$

provided $(z - z_1) \gg r_0$ and $(z - z_1) \ll a$.

For $(z - z_1)$ not small compared to a, (i.e., circuit radius not awfully large) the field would drop even faster with $(z - z_1)$ due to the shielding effect of the circuit. On the other hand, very near to the beam element $(z - z_1 \ll r_0)$, the field is approximately that of a disc, which is nearly independent of z, i.e.,

$$E = \text{Const}\cdot\frac{q\Delta z}{\pi r_0} \tag{8}$$

independent of z for $z \ll r_0$.

Thus to a fair approximation the space charge field may be considered to be uniform for an axial distance of the order of a half a beam radius, and to drop rapidly at greater distances. For a given current element, a small diameter beam has an intense field extending only a short distance, while an equal charge element in a larger beam has a weaker longitudinal field extending to a greater distance.

At low amplitudes the extent of the forces makes no difference in operation, for a sinusoidal current gives a sinusoidal space charge field in either case. However, at large amplitudes, a sharp change in current density has a very high short range space charge field if the beam is small, or a much smaller smoothed out long range field if the beam is large. For $\gamma r_0 = 0.5$ which appears to be an optimum compromise between the effects of space charge and field non-uniformity, the space charge field could scarcely be confined closer than about $\pm 30°$ in phase. On the other hand, a sharp bunching of electrons in a beam having

$\gamma r_0 = .05$ would have 100 times the space charge field, extending however only one tenth as far from the current discontinuity.

Returning to Fig. 9 we can see how these considerations enter into the development of the beam modulation. In the case of the small beam, Fig. 9(c), at the very beginning of the formation of a cusp, the strong highly concentrated space charge force causes a rapid deceleration of nearby electrons, resulting in the relatively early formation of a diminutive tail. The very high localized space charge force also prevents as tight bunching of electrons, forcing some to move forward and continuously repopulate the accelerating part of the wave. The relatively early falling apart of the initial bunch and the greater acceleration of the overriding electrons evidently give the latter enough velocity to penetrate the main bunch of electrons and form the second class of electrons in the main bunch, 90°–150° in Fig. 9(c). Thus the net result of reducing the beam size is a severe aggravation of space charge debunching effects, with a consequent reduction in efficiency. To get high efficiency, we conclude, the beam should not be small. It should not be larger than $\gamma r_0 = 0.7$ however, for then the circuit field is not uniform enough over the beam cross-section to excite it properly, resulting in a loss in efficiency as is evident in Figs. 2 and 3.

EFFECT OF INCREASED BEAM VOLTAGE

It is common practice in the operation of traveling wave tubes to elevate the beam voltage, taking a sacrifice in gain in order to obtain increased power output. The effects on the beam modulation are shown in Fig. 10. In Fig. 10(a), the voltage is somewhat below that giving maximum gain. The curve is characteristic of what we have already seen but the bunching is less pronounced and the velocities are less reduced. In Fig. 10(b) the voltage is somewhat above that giving maximum gain and the curve is much like that of Fig. 8 except that the decelerated electrons are slowed by a greater amount, consistent with the increased separation of electron and wave velocity, and also with the measured increase in power output.

Increasing the beam voltage still further gives only a slight increase in efficiency. Fig. 10(c) shows that even though electrons are slowed to still lower velocities, and the velocity spread is increased, many more electrons override the circuit wave and are accelerated, thereby offsetting the greater contribution of the slower electrons. This is much like what was seen with increasing space charge (QC) and indeed the effects are almost equivalent. As one would expect therefore, little is gained by elevating the beam voltage if the space charge is large, the

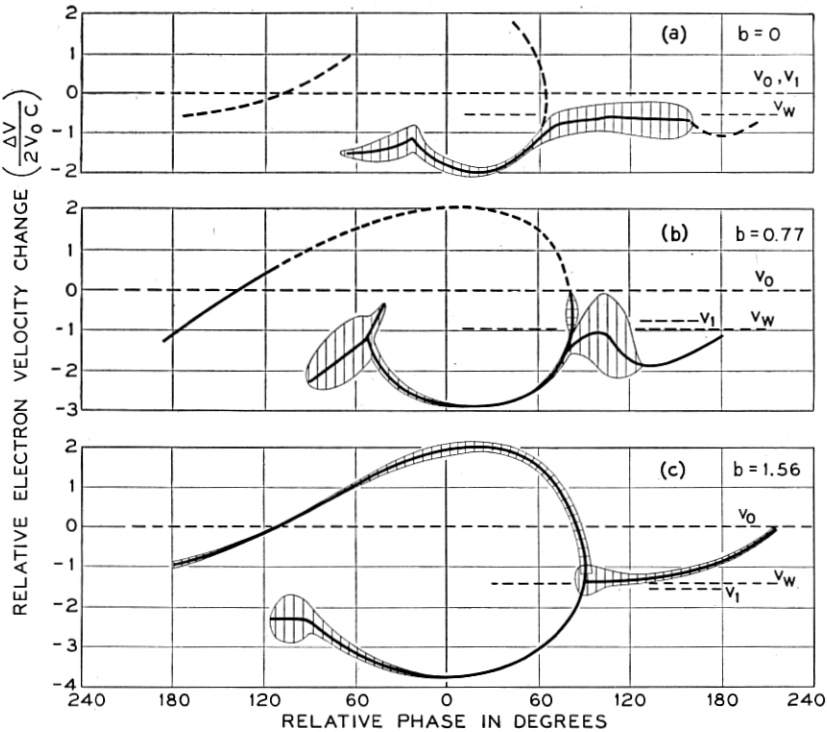

Fig. 10 — The influence of beam velocity on ac velocity and current. When the velocity is raised too high, the electrons are not effectively trapped by the wave, and override into the accelerating field. With large QC and/or small γr_0 the electrons override in any case, and little is gained by increasing b. For this case $QC = 0.13$ and $\gamma r_0 = 0.21$.

main effect being to push more electrons forward into the accelerating region.

ELECTRIC FIELD IN THE BEAM

Besides telling a clear story of the non-linear dynamics of the traveling wave tube, the foregoing curves contain a lot of information about average current and velocity distributions. From the current or velocity curves we can in turn deduce the distribution of longitudinal electric field in the beam. Figs. 11(a) and (b) show the instantaneous current as a function of phase, taken from the curves of Figs. 8(a) and (b). The infinite differential in the velocity curve necessarily gives a pole in the charge density (at about 88°). The total charge in the vicinity of the

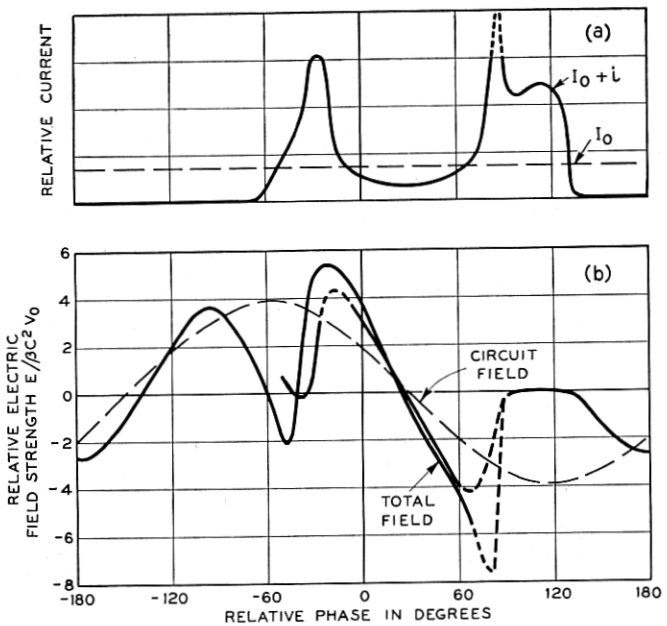

FIG. 11 — AC current and electric field in the beam. The upper curve comes directly from Fig. 8(a). The lower curve is deduced by an approximate method from the velocity curve of Fig. 8(a). The double value below 90° is partly due to inconcistency between the two parts of the velocity curve, and partly due to the nature of the approximation.

pole, and the range of the space charge force (dependent upon QC and γr_0) determines its effect upon the electron dynamics.

Most of the current is incorporated in the two bunches nearly 180° apart, as we have seen, each bunch having a current density many times the average.

We might obtain the space charge fields from the current density, but this would require a rather definite knowledge of the characteristic space charge field versus distance as influenced by beam diameter. It would also be pushing the accuracy of charge density measurement, which is crude at best. A better way is to compute the electron acceleration from the velocity curves. This may be done by taking two velocity patterns at slightly different signal levels, and tracing electrons from one to the next, using the measured velocity to determine the relative phase shift of any electron.

In the appendix it is shown that a close approximation to this is

$$E_\Phi = 2\beta C^2 V_0 \left[\frac{(V_0 - V_w) + \Delta V}{2V_0 C}\right] \frac{d}{d\Phi}\left(\frac{\Delta V}{2V_0 C}\right) \qquad (10)$$

where the parameters are all obtained from a single velocity curve, and

E_Φ is field strength in volts meter at phase Φ

$\frac{\Delta V}{2V_0C}$ is the value of the ordinate of the velocity characteristic of of interest (Figures 7 to 10) and

$\left(\frac{V_0 - V_w}{2V_0C}\right)$ is the value of the ordinate corresponding to the wave velocity. (To be precise, the wave velocity at the associated output level, but to a reasonable approximation, that of the wave velocity at low levels. (This value is indicated by V_w in the velocity curves.)

The total electric field has been computed for the case of Figs. 8(a) and (b) and is given in Figs. 11(b) and 12(b) together with the circuit field calculated for the associated power level and plotted with an arbitrarily chosen phase. In each case it is seen that the space charge field is comparable in magnitude to the circuit field, is far from sinusoidal, and

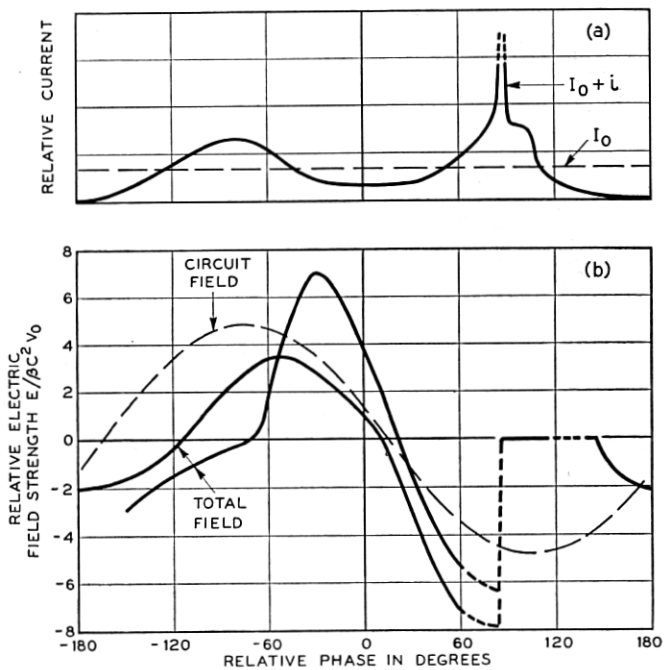

Fig. 12 — AC current and electric field in the beam deduced from Fig. 8(b). The greater space charge results in a less defined bunch, and smoother space charge field than in Fig. 11.

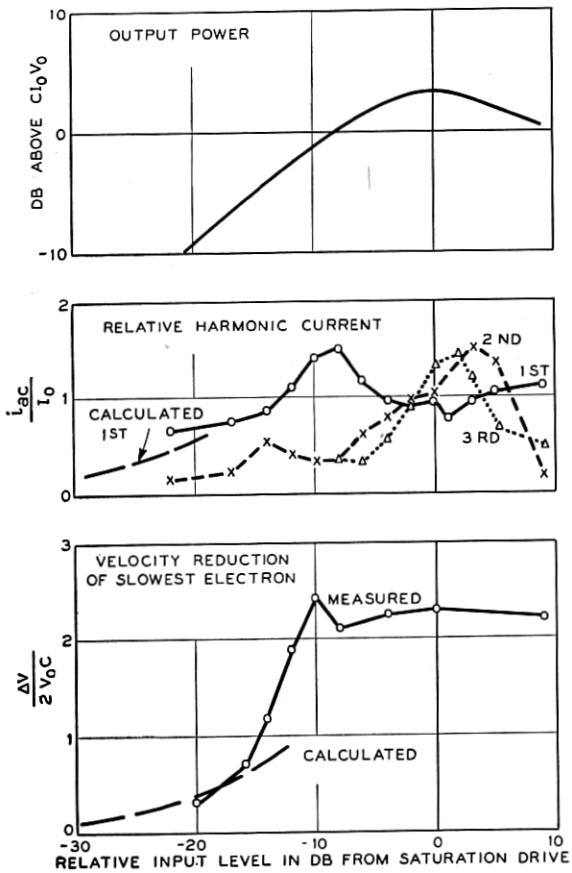

Fig. 13 — Curves of output level, fourier component amplitudes of beam current, and peak velocity as a function of input level for low space charge. These curves were deduced from Fig. 8(a).

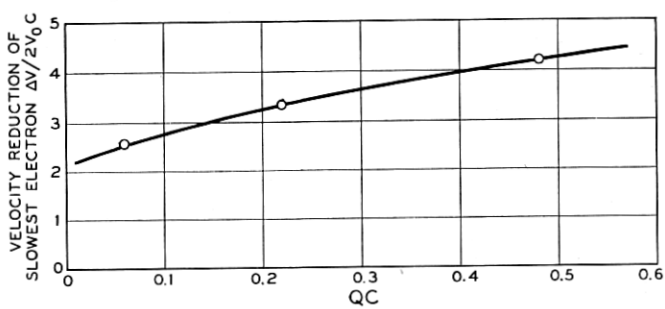

Fig. 14 — Maximum velocity reduction as a function of space charge (from Fig. 8). The velocity reduction is about 3.5 y_1 .

agrees qualitatively with what would be expected from the associated curve of beam current.

To determine the curves of Figs. 11 and 12 is rather stretching the accuracy of the measurements as can be seen by the large discrepancy in the field calculated from the two parts of the velocity curve which of course should be identical. The figures do give an interesting qualitative picture of traveling wave tube behavior however, and are included here for that reason.

OVERALL VELOCITY SPREAD

Of more practical importance is the overall velocity spread in the spent beam. It is often desirable to reduce the power dissipation in a traveling wave tube by operating the collector at a potential below that of the electron beam, and it is interesting to see how far one might go. Fig. 13 shows how the velocity reduction of the slowest electron, together with the output level and fourier current components of beam current vary with input level. For small amplitudes, the low level theory accurately predicts the velocity, but near overload, as we have seen, the minimum velocity drops sharply to a value several times lower than that projected from small signal theory.

The maximum velocity spread dependence upon the space charge parameter QC is shown in Fig. 14. Similar data for values of the other parameters may be obtained from the velocity diagrams.

From the foregoing data, one can deduce the amount of reduction of collector potential that should be theoretically possible without turning back any electrons. An idealized unipotential anode could collect all the current at a potential ΔV (in the foregoing figures) above the cathode, decreasing the dissipated power by a factor of $\Delta V/V_0$ below the dc beam power.

STOPPING POTENTIAL MEASUREMENTS

Information on spent beam velocity has also been obtained by a stopping-potential measurement at the collector of a more conventional 4,000-mc traveling wave tube.* Two fine mesh grids were closely spaced to a flat collecting plate, and collector current was measured as a function of the potential of second grid. The first grid was very dense, to prevent reflected electrons from returning into the helix. One curve taken with this arrangement is shown in Fig. 15 and for comparison we have

* Similar measurements have been reported by Atsumi Kondo, Improvement of the Efficiency of the Traveling Wave Tube, at the I.R.E. Annual Conference on Electron Tube Research, Stanford University, June 18, 1953.

plotted the distribution predicted from Fig. 9(b). The *RF* losses in the 4,000-mc tube were not negligible, and probably account for slightly smaller power output and greater proportion of higher velocity electrons.

COMPARISON WITH COMPUTED CURVES

Non-linear calculations of traveling wave tube behavior have been made by Tien, Walker and Wolontis[7] and by Tien[9] covering the same region of parameter values as is reported here. In Figs. 2, 3, 4 and 9 are shown some of their data on our coordinates. The similarity of the results over much of the range is rather reassuring. It is interesting that in order to make the computations it was necessary to assume two space charge factors, just as was found experimentally. There are, however, some significant differences:

1. In general, the computed values give a higher value of efficiency than is measured, by about 25 per cent. Thus, the computations indicate

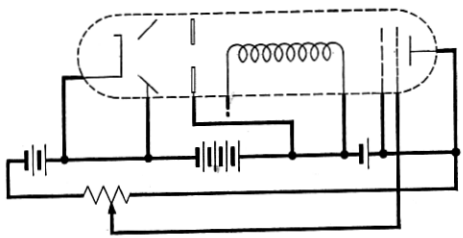

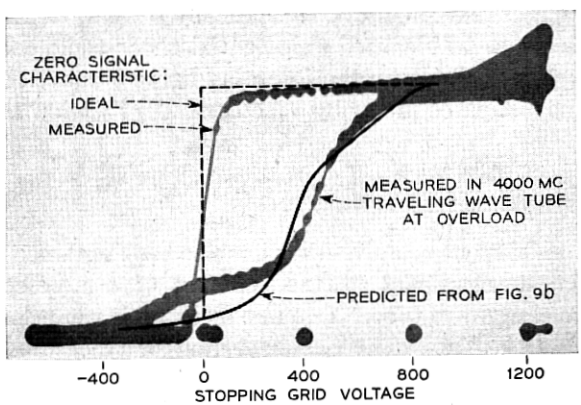

Fig. 15 — Collected current versus stopping potential. The oscilloscope curve is for a 4,000-mc tube, and the other that predicted from the scale model measurements. By integrating current as a function of velocity for Figs. 7–10 stopping potential distributions can be deduced for other conditions.

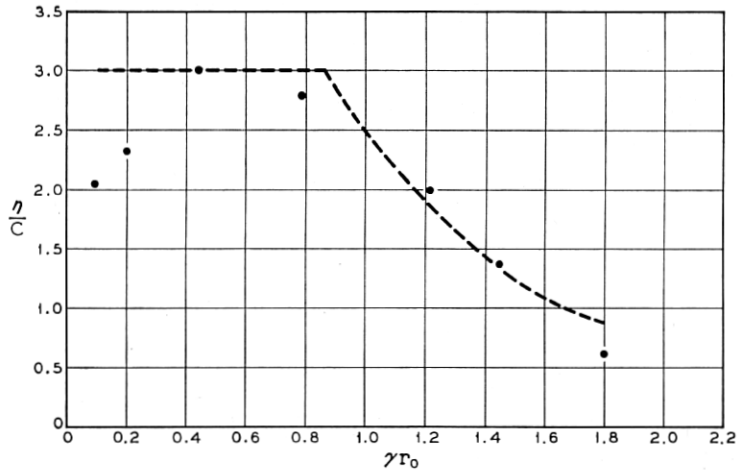

Fig. 16 — Efficiency versus γr_0 for small QC. The dashed curve is proportional to the amount of beam current in the circuit field strength having at least 85 per cent of the intensity at the edge of the beam. This illustrates the fact that for large beams only the edge of the beam is effective.

that with the reasonable values of $QC = .25$ and $\gamma r_0 = 0.8$ ($k_T = 2.5$), the efficiency would be about $3.8C$, whereas the measured value is $3.1C$.

2. The largest discrepancy in the measured and computed value of η/C is for large values of γr_0 (small k_T), where the computations show a steady increase in efficiency instead of a sharp decrease. This arises because the computational model assumed the electric field to be uniform across the beam, whereas in the actual tube it varies as $I_0(\gamma r)$, and for large values of γr_0 the field is weak near the beam axis. This effect is shown in Fig. 16 where η/C is plotted versus γr_0 for small values of QC, on the same scale with a curve proportional to the square of the fraction of the beam within a cylindrical shell such that

$$1 - \frac{I_0(\gamma r_1)}{I_0(\gamma r_0)} = 0.85 \tag{11}$$

where r_1 is the inside radius, and r_0 the outside beam radius (i.e., the fraction of the beam in a field greater than 85 per cent of that at the beam edge).

No serious studies of velocity were made for large beams, but on cursory examination it was evident that the beam modulation varied considerably over the cross section when the beam was very large, and scarcely at all when it was smaller than around $\gamma r_0 < 0.8$.

3. The observed effect of small beam radius upon efficiency is not as pronounced as was found in the computations. The reason is not known but may be due to modulation of the beam diameter at large signal levels. This effect would be negligible with the larger γr_0's, due to the focusing fields being relatively much larger.

4. The computations, and also those of Nordsieck,[5] Poulter[6] and Rowe[8] indicate a much higher efficiency than has been observed at elevated beam voltages and small C and QC. The reason for this may be that the limited number of "electrons" used in the computational models fail to adequately account for the very sharp space charge cusp that forms under low QC conditions, or that interpolation between their points should not be linear, as assumed in making the comparison. On the other hand it would be difficult to be sure that nonuniformities in electron emission were not influencing the measurements in the case of the large beams by giving a larger QC than calculated.

5. The increase in efficiency to be had by elevation of beam voltage is much smaller than is indicated by the computations. This may be a real difference, or it may be that at elevated voltages, the measurements are beginning to feel the influence of overloading in the attenuator. The margin of safety on attenuator overloading is not as great as one would like at the higher frequencies.

6. The velocity curves, Fig. 8, compare the computed and measured data on three runs. For small QC, Fig. 8(a), the agreement is remarkably good considering the fact that in the computation only 24 "electrons" were used to describe a rather complicated function. The effect of the lumping of space charge in the artificial 'disc' electrons causes a scatter of points which is different from that in an actual tube as is especially apparent in Figure 8c. In spite of this the computational results indicate a velocity spread and current distribution not greatly different from that observed.

CONCLUSIONS

The large scale model traveling wave tube is a means for the determination of non-linear behavior, and has been valuable in determining relationships and limitations important to efficient operation of such tubes. It has shown that there is a broad optimum in tube parameters around $C = 0.14$ $QC = 0.2$ and $\gamma r_0 = 0.5$ for which values it is possible to obtain efficiencies well above 30 per cent. The measured ac beam velocity and current near overload show that it is unlikely that significant increase in efficiency can be obtained by any simple expedients such

as operations on the helix pitch alone, or the use of an auxiliary output circuit.

The results being in normalized form, are believed to be generally applicable to conventional traveling wave tube design. With determination of an equivalence in beams, they should even be a useful guide in the design of tubes using hollow beams or other configurations.

The work described could not have been done without the able assistance of G. J. Stiles and L. J. Heilos and the helpful council of many of my colleagues at Bell Telephone Laboratories.

Appendix

Scale model tube design

There were a larger number of factors to be accounted for in the design of this tube. Its proportions should be such as to make it representative of the usual design of traveling wave tube. Its size should be such as to make it easy to define the electron beam boundary, and to dissect the beam. The size should also be such that the electron beam velocity analysis could be done before the beam character would be changed either by space charge, or its velocity spread. The voltage should be low so that further acceleration in the velocity analyzer would not lead to an inconveniently high voltage. Finally, the availability of suitable measuring gear over a 3–1 frequency range, and the size of the laboratory must be considered. All of these factors led to low frequency operation, limited principally by the laboratory size and the mechanics of construction.

A moderate perveance of around 0.2×10^{-6} was taken, with a γa of 1.2 and γr_0 of 0.8 in a representative helix with small impedance reduction due to dielectric and space harmonic loading. This is representative of practical tube design in the microwave range and is centered on the parameter values of most general interest. At a frequency of 100 mc and a beam potential of 400 volts this resulted in a helix 10 feet long and 1½ inches in diameter, with an electron beam 1 inch in diameter. The choice of frequency was finally determined by the availability of measuring equipment, and the voltage was selected to give a convenient size for dissection of the electron beam.

By changing frequency, beam current, and beam diameter it was possible to cover a reasonable range of γr_0, and QC, and to make some observations into the region of large C operation.

In all of the measurements described, a very strong uniform magnetic field was used to confine the beam, and therefore scaling of the magnetic

focusing field need not be considered. The electron beam was produced in a gridded gun and is thus near to the ideal confined flow, which is the only focusing arrangement which is known to determine a reasonably uniform boundary to the beam. The beam size and straightness was checked using a fluorescent screen at the collector end.

NORMALIZING FACTORS

The measurements described are expressed relative to the linear theory, in Pierce's[2] notation, which are generally used in the design of traveling wave tubes. Thus, instead of being presented in the terms of measurement or simply normalized to efficiency, perveance, impedance, etc., they are expressed in terms of C, QC, γr_0, etc., with normalized fields, currents and velocities. In this way the results become adjuncts to the linear theory and are more easily applied to tube design. Electron velocity is plotted on the same scale as the relative velocity parameters b and y_1 used in low level theory, (i.e., normalized to $\Delta V/2V_0C$). Efficiency is normalized as η/C, which for C less than 0.1 is relatively independent of C. Field strength in the linear region is proportional to

$$\sqrt{\frac{\eta'}{C}}$$

(η' being efficiency measured at the appropriate signal level). Solving the equation for C^3,

$$C^3 = \frac{E^2}{2\beta^2 P}\frac{I_0}{2V_0} \tag{12}$$

gives us

$$\sqrt{\frac{\eta'}{C}} \approx \frac{E}{\beta C^2 V_0} \tag{13}$$

which we use as the normalizing parameter for electric field. Circuit potential is the integral of circuit field over a quarter period, giving a normalized parameter V/V_0C^2. For convenience in the use of common coordinates, circuit potential was plotted as $-V/2V_0C^2$ in Figure 7.

The other curves are plotted as values relative to dc quantities or to saturation level.

Strictly speaking, the results hold only for tubes having the same proportions as the model. Practically, however, as long as the helix impedance and radius (ka or γa) are not different by orders of magnitude from the values used, and as long as the perveance is low (below 2×10^{-6} for

instance), the results are believed to be significant for tubes having the indicated values of γr_0 and QC.

HELIX IMPEDANCE

It is important to the measurements to have an accurate evaluation of the helix impedance. Several methods of measurement have been discussed in the literature.[21, 22] That described by R. Kompfner was selected, wherein the circuit impedance is correlated with the beam current and voltage which gives a null in the output signal. When the beam voltage and current are adjusted to give zero transmission for a lossless section of helix (neglecting space charge) $CN = 0.314$ and $\delta V/V_0 \cong 1/N$. Using the measured length of the helix, and measuring the voltage and current giving the null in signal transmission, we can compute C, and thus the impedance and velocity (synchronous voltage) of the helix.

The impedance was calculated by P. K. Tien,[23] and the results are compared in Fig. 17. The measured impedance at the high frequency end was much too low until space charge in the beam was accounted for in interpreting the measurements. Fortunately, in the absence of attenu-

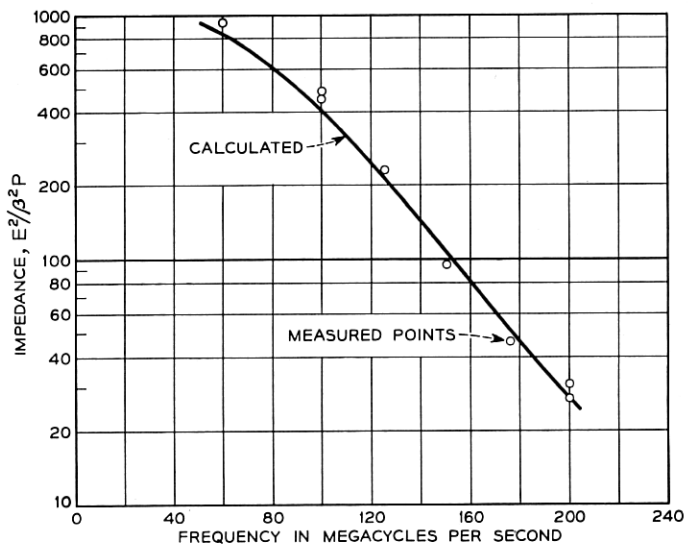

Fig. 17 — Helix impedance as a function of frequency. The impedance was calculated taking into account dielectric loading and wire size. It was measured using the Kompfner dip method, taking account of space charge.

ation, the conditions for start of oscillation in a backward wave oscillator are the same as for the output null in a traveling wave tube. Space charge was first accounted for using the results of H. Heffner[24, 25] giving an excellent check between predicted and computed helix impedance. Later C. F. Quate[26] showed that the same measurement could be used to determine the space charge parameter QC as well as the helix impedance. Since thermal velocity effects and the uncertainty of some of the assumptions used in evaluating the small signal effects of space charge cast some doubt on the proper evaluation of this term, further measurements were made on this factor, and a satisfactory correlation between the observed value of QC and that computed from the Fletcher[27] curves was obtained.

TOTAL ACCELERATING FIELDS

From the velocity characteristics shown in Figs. 7 through 10, we can deduce the electron accelerations, and thus the electric fields at any point. While the curves are actually diagrams of velocity as a function of phase, they closely correspond to the velocity-time or distance distribution of the electrons in the traveling wave tube. Knowing these characteristics we can deduce the motion of any element of charge, and thus the force under which it moves. It is observed that over most of the curve the shape of the velocity pattern does not change nearly so rapidly as the redistribution of electrons within the pattern. Thus, we can approximate the situation at any amplitude by assuming the velocity pattern to be constant, and that electrons move within the pattern according to simple particle dynamics. This is a good approximation except where the acceleration is high (i.e., vertical crossings of the wave velocity line).

Consider then an element of the velocity pattern at phase Φ_1 and velocity $(u_0 + \Delta u)$. In an interval dt this element will move a distance

$$(u_0 + \Delta u)\, dt \tag{14}$$

and will change velocity by

$$du = E \frac{e}{m} dt \tag{15}$$

At the same time the wave will have moved a distance $v\, dt$, resulting in a relative change in phase between wave and current element of

$$d\Phi = \beta(u_0 - v + \Delta u)\, dt \tag{16}$$

In terms of equivalent differences the term in brackets can be written

$$(u_0 - v + \Delta u) = \sqrt{2 \frac{e}{m} V_0}\, C \left(\frac{V_0 - V_w + \Delta V}{2 V_0 C} \right) \tag{17}$$

from (16) and (17) we can write:

$$\frac{du}{dt} = \frac{du}{d\Phi}\frac{d\Phi}{dt}$$
$$= \frac{d}{d\phi}\left(\frac{\Delta V}{2V_0C}\sqrt{2\frac{e}{m}V_0}\,C\right)\left[\beta\sqrt{\frac{e}{m}V_0}\,C\left(\frac{V_0 - V_w + \Delta V}{2V_0C}\right)\right] \tag{18}$$

giving (from 15)

$$\frac{E}{\beta V_0 C^2} = 2\left[\left(\frac{V_0 - V_w}{2V_0C}\right) + \left(\frac{\Delta V}{2V_0C}\right)\right]\frac{d}{d\Phi}\left(\frac{\Delta V}{2V_0C}\right) \tag{19}$$

β, V_0 and C are constants of the tube, the first inner parenthesis may be calculated from the tube constants and is shown in the curves. $\Delta V/V_0C$ and its differential are the value and the slope of the velocity curve in question.

The important approximations here are that the velocity-phase curves are representative of velocity-distance characteristics, which is true for small values of C, and that the electrons move roughly tangent to the given velocity pattern. By comparing several patterns at different signal levels it is observed that this is true to a fair accuracy over most of the curve. Also it is assumed that the wave velocity at large amplitudes is the same as that for small signals, which is not quite true. The resulting curves give at least a qualitative picture of the field distribution within a traveling wave tube, and serve to emphasize the importance of space charge fields in determining the non-linear characteristics.

ELECTRIC FIELD OF THE HELIX WAVE

In order to see what part of the field is due to space charge we must evaluate the corresponding helix fields. A value for this can be derived from the basic traveling wave tube equations assuming the helix fields to be sinusoidal and not seriously affected in impedance by the beam (small C again). By definition

$$\frac{E^2}{2\beta^2 P}\frac{I_0}{4V_0} = C^3 \tag{18}$$

and

$$\frac{\eta'}{C} = \frac{P}{I_0 V_0 C} \tag{19}$$

where η' is normalized power level, i.e., efficiency corresponding to the signal level E of interest. From this we deduce for the normalized circuit

field

$$\frac{E}{\beta V_0 C^2} = 2\sqrt{2}\sqrt{\frac{\eta'}{C}} \tag{20}$$

which integrates to give a normalized ac circuit voltage

$$\frac{V}{2\sqrt{2}V_0 C^2} = \sqrt{\frac{\eta'}{C}} \tag{21}$$

RELATIVE PHASE BETWEEN WAVE, VELOCITY AND CURRENT

The velocity analyzer provides no convenient measure of relative phase between the helix wave and the beam modulation. Therefore we compute the relation of helix field and beam modulation for a small signal, and for large amplitudes measure the phase of each relative to that at small amplitudes.

Pierce gives the relationship[2] $$v = \frac{-\eta\Gamma V}{u_0(j\beta_e - \Gamma)} \tag{22}$$

which using (9) and the fact that $$\beta_e C\delta = j\beta_e - \Gamma \tag{23}$$

gives for the small signal beam modulation

$$\frac{\Delta V}{2V_0 C} = -j\frac{\sqrt{2}}{\delta}\sqrt{\frac{\eta}{C}} = \frac{\sqrt{2}}{|\delta|}\sqrt{\frac{\eta'}{C}}\underline{\left|\left(\tan^{-1}\frac{y_1}{x_1}\right) - \frac{\pi}{2}\right.} \tag{24}$$

Similarly we have for the small signal current modulation

$$i = I_0\sqrt{2\frac{\eta}{C}}\cdot\delta^2 = I_0\sqrt{2\frac{\eta}{C}}\,|\,\delta^2\,|\,\underline{\left|2\tan^{-1}\frac{x_1}{y_1}\right.} \tag{25}$$

The value of $\delta(= x_1 + jy_1)$ is given in Fig. 18, drawn from data supplied by P. K. Tien, from Pierce[2] and from Birdsall and Brewer.[28] This figure was also used as a basis for determining the values of y_1 and b used in several of the curves.

MEASUREMENT OF POWER

The output power, and relative output phase was measured using a micro-oscilloscope.[29] The subharmonic of the signal was used for a sweep voltage, and phase was measured from the shape of the observed lissajou figures. The oscilloscope deflection was compared with the dc deflection from a battery standard, and checked on occasion with a bolometer power meter at the operating frequency.

THE VELOCITY ANALYZER

There are many ways in which one may separate velocities in an electron stream. Crossed electric and magnetic fields were used in this ex-

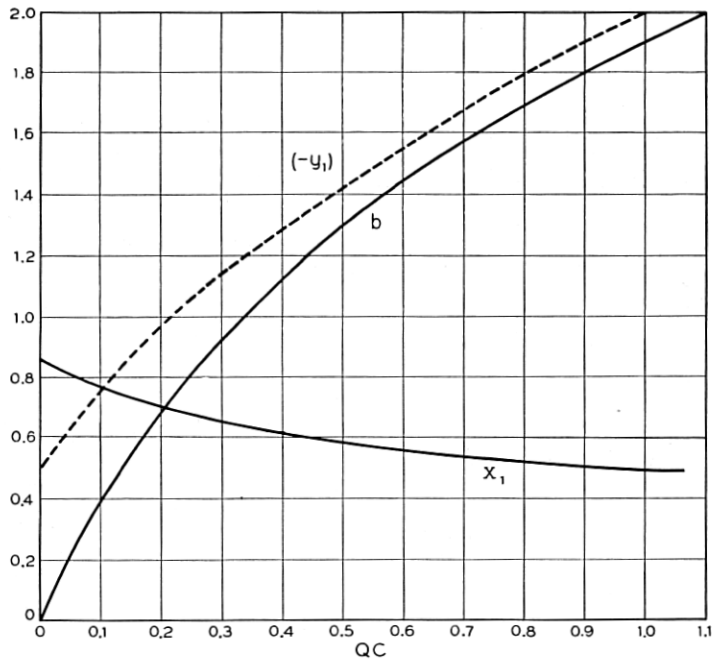

Fig. 18 — Increasing wave propagation factors used in interpreting the measurements. These are the maximum value of x_1 and the corresponding value of b and y_1 for given values of QC.

periment because a simple control of sensitivity was important in order to study velocity differences ranging from 1 per cent up to as much as 100 per cent of the dc beam velocity.

The velocity analyzer is sketched in Fig. 5. It consists of an aperture which transmits only a few microamperes of the electron stream; a magnetic pole piece (not shown) terminating the focusing field; a pair of horizontal deflection plates; an electrostatic lens system; pole pieces and deflection plate to provide a region with crossed electric and magnetic fields; and finally a drift tube, a post deflection acceleration electrode and fluorescent screen. The whole assembly is raised 1,000 volts above the helix potential and the 0.001″ aperture is very close to the end of the helix, so that the electrons are very quickly accelerated to a high voltage. By this means, the region of debunching outside of the helix field is kept below 1.4 radians transit angle and the velocity spread within the analyzer is reduced by a factor of four. Space charge within the analyzer is entirely negligible because of the small current transmitted.

In order to discriminate in phase before the electrons are scrambled

due to their spread in velocity, the horizontal sweeping plates are mounted just as close to the aperture as is deemed practical. The observed velocity spreads in the beam were such as to give less than 0.2 radians error in phase under the worst conditions.

The horizontal deflecting plates were driven synchronously with a sub-harmonic of the RF input to the helix, and the resulting deflection served to separate electrons according to phase in the final display.

Placing the focusing lens after the deflection plates results in a considerable reduction in deflection sensitivity. However, undesirable magnification of the pinhole aperture dictated that the lens could not be close to it, and it was important to initiate the deflection as early as possible. The lens consists of three discs, the center one being biased to about 800 volts above the mean voltage of the rest of the system.

Immediately after the lens there are two iron pole pieces and two insulated electric deflection plates which extend parallel to the beam for 1¼ inches. The pole pieces provide a dc magnetic field up to about 20 gausses induced by small coils outside of the envelope, and the electric deflection plates are biased with up to a corresponding 50 volts dc polarized to oppose the magnetic deflection of the beam. The electric and magnetic fields are adjusted so that the normal unmodulated electron beam traverses the region with no deflection and strikes the center of the fluorescent screen. In the crossed field region

$$\frac{E}{B} = \sqrt{2\frac{e}{m}V_0}. \tag{26}$$

Electrons having greater or lesser velocity are deflected parallel to the electric field, and give a corresponding deflection from the center of the fluorescent screen.

To get a display in which the various elements are not hopelessly entangled, it was necessary to sweep the trace in an initial ellipse at a subharmonic rate. The sweep voltage was applied to the horizontal deflection plates, with just a little applied to the vertical plates through a phase shifter. The relative phase of any part of the trace was measured from the ellipse, and the velocity sensitivity was calibrated by observing the ellipse deflection as a function of the dc beam potential, as shown in Fig. 6(a). There is a small error due to the sensitivity of deflection to velocity, and due to distortion of the ellipse by fringing fields.

In order to measure velocity and current density in the displayed pattern, the fluorescent screen was photographed, and the negative projected in a microcomparator. It was assumed that with the small currents used, the light intensity was proportional to current, and the film linearity was calibrated by making exposures of several different durations. The trace density was measured with a densitometer, sweeping

over the trace width to account for variations in focus for different parts of the pattern. Admittedly, the process is not very accurate, but it does give a rough measure of current density and helps considerably in interpreting the observed velocity patterns.

NOMENCLATURE

a	Circuit radius
b	Parameter relating electron velocity to that of the cold circuit wave $u_0 - v_1/u_0C = \Delta V/2V_0C$
B	Magnetic field
β	the axial phase constant ω/v_1
C	The gain parameter $= (E^2/2\beta^2P)\ (I_0/4V_0)$
γ	Radial phase constant $\cong \beta = \omega/v_1$
δ_1	Complex propagation constant for the increasing wave
E	Electric field
E_Φ	Electric field at phase Φ
e/m	Charge to mass ratio of the electron
I_0	Beam current in amperes
$I_0(\ )$	Modified Bessel function
k_T	Tien's constant k, $= 2/\gamma r_0$
ka	Circuit circumference measured in (air) wavelengths
N	Number of wavelengths
η	Maximum efficiency
η'	Efficiency at an intermediate power level
P	RF power obtainable from the circuit
QC	Space charge parameter
q	Charge per unit length in the electron beam
r	Radial distance from the axis
r_0	Beam radius
t	Time variable
u	Electron velocity
u_0	DC beam velocity
v	AC velocity of the electron beam
v_1	Wave velocity
V_0	DC beam voltage
T_w	Voltage corresponding to the wave velocity
ΔV	Voltage difference corresponding to the difference in velocity of an electron and the dc beam velocity
δV	Difference between synchronous voltage and that giving the Kompfner dip
Φ	Relative phase
z	Distance measured along the beam

REFERENCES

1. Pierce, J. R., Theory of the Beam Type Traveling Wave Tube, Proc. I.R.E., **35,** pp. 111–123, Feb., 1947.
2. Pierce, J. R., Traveling Wave Tubes, D. VanNostrand Co., Chapter XII.
3. Slater, J. C., Microwave Electronics, D. VanNostrand Co., 1950, pp. 298.
4. Brillouin, L., The Traveling Wave Tube (Discussion of Waves of Large Amplitudes), J. Appl. Phys., **20,** p. 1197, Dec., 1949.
5. Nordsieck, A., Theory of the Large Signal Behavior of Traveling Wave Amplifier, Proc. I.R.E., **41,** pp. 630–647, May, 1953.
6. Poulter, H. C., Large Signal Theory of the Traveling Wave Tube, Tech. Report No. 73 Electronics Research Laboratory, Stanford University, Stanford, California, Jan., 1954.
7. Tien, P. K., Walker, L. R., and Wolontis, V. M., A Large Signal Theory of Traveling Wave Amplifiers, Proc. I.R.E., **43,** pp. 260–277, Mar. 1955.
8. Rowe, J. E., A Large Signal Analysis of the Traveling Wave Amplifier, Technical Report No. 19, Electron Tube Laboratory, University of Michigan.
9. Tien, P. K., A Large Signal Theory of Traveling Wave Amplifiers Including the Effects of Space Charge and Finite C, B.S.T.J., **34,** Mar., 1956.
10. Brangaccio, D. J., and Cutler, C. C., Factors Affecting Traveling Wave Tube Power Capacity, Trans. I.R.E. Professional Group of Electron Devices, **PGED 3,** June, 1953.
11. Crumly, C. B., Quarterly Status Progress Report No. 26, Electronics Research Laboratory, Stanford University, Stanford, California, pp. 10–12.
12. Doehler, O., et Kleen, W., Phenomènes non Linéaires dans les Tubes a Propagation D'onde" Annales de Radioélectricité (Paris), **3,** pp. 124–143, 1948.
13. Doehler, O., et Kleen, W., Sur le Rendement du Tube a Propagation D'onde," Annales de Radioélectricité, Tome IV No. 17 Juillet, 1949 pp. 216–221.
14. Berterotiére, R., et Convert, G., Sur Certains Effets de la Charge D'espace dans les Tubes a Propagation D'onde, Annales de Radioélectricité, Tome V, No. 21, Juillet, 1950.
15. Klein, W., und Friz, W., Beitrag zum Verhalten von Wanderfeldrähren bei Hohen Engangspegeln, F.T.Z., pp. 349–357, July, 1954.
16. Warnecke, R. R., L'évolution des Principes des Tubes Électroniques Modernes pour Micro-ondes, Convegno di Elellronica e Televisione, Milano, p. 12–17, Aprile, 1954.
17. Warnecke, R. R., Sur Quelques Résultats Récemment Obtenus dans le Domaine des Tubes Electroniques pour Hyperfréquences, Annales de Radioélectricité, Tome IX, No. 36, Avril, 1954.
18. Warnecke, R., Guenard, P., and Doehler, O., Phénomènes fondamentaux dans les Tubes à onde Progressive, Onde Electrique, France, **34,** No. 325, p. 323–338, 1954.
19. Brück, L., und Lauer, R., Die Telefunken Wanderfeldröhre TL6, Die Telefunken-Röhre Heft 32, pp. 1–21, Februar, 1955.
20. Brück, L., Vergleich der Verschiedenen Formeln für den Wirkungsgrad einer Wanderfeldröhre, Die Telefunken-Röhre Heft 32, pp. 23–37, Februar, 1955.
21. Cutler, C. C., Experimental Determination of Helical Wave Properties, Proc. I.R.E., **36,** pp. 230–233, Feb., 1948.
22. Kompfner, R., On the Operation of the Traveling Wave Tube at Low Level, Journal British I.R.E., **10,** p. 283, Aug.-Sept., 1950.
23. Tien, P. K., Traveling-Wave Tube Helix Impedance, Proc. I.R.E., **41,** pp. 1617–1623, Nov., 1953.
24. Heffner, H., Analysis of the Backward-Wave Traveling-Wave Tube, Proc. I.R.E., **42,** pp. 930–937, June, 1954.
25. Johnson, H. R., Kompfner Dip Conditions, Proc. I.R.E., **43,** p. 874, July, 1955.
26. Quate, C. F., Power Series Solution and Measurement of Effective QC in Traveling-Wave Tubes, Oral presentation at Conference on Electron Tube Research, University of Maine, June, 1954.
27. Fletcher, R. C., Helix Parameters in Traveling Wave Tube Theory, Proc. I.R.E., **38,** pp. 413–417, Apr., 1950.
28. Birdsall, C. K., and Brewer, G. R., Traveling Wave Tube Characteristics for Finite Values of C, Trans. I.R.E., **PGED-1,** pp. 1–11, Aug., 1954.
29. Pierce, J. R., Traveling Wave Oscilloscope, Electronics, **22,** Nov., 1949.